EMC3-EIRENE implementation on NCSX and first applications

F. Sardei [1)], A. Brooks [2)], Y. Feng [1)], F. Herrnegger [1)],T. Kaiser [3)], J. Kisslinger [1)], R. Maingi [4)], D. Monticello [2)], M.C. Zarnstorff [2)]

[1)] *Max-Planck-Institut für Plasmaphysik, Euratom Association, Greifswald/Garching, Germany*
[2)] *Princeton Plasma Physics Laboratory, Princeton, USA*
[3)] *Lawrence Livermore National Laboratory, Livermore, USA*
[4)] *Oak Ridge National Laboratory, Oak Ridge, USA*

The paper presents the status of the implementation of the EMC3-EIRENE code on NCSX. Particular attention is devoted to the construction of the 3D plasma computational grid in the SOL, which consists of a 2D radial-poloidal system of finite flux tubes extending half a field period. In a first application, the code simulates the energy transport for electrons and ions in a typical SOL configuration bounded by model target plates. The distribution of connection lengths defined by the plates and the resulting temperature profiles are shown and discussed.

Keywords: stellarator, NCSX, divertor, transport, 3D modeling, EMC3-EIRENE code

1. Introduction

In helical devices, SOL plasmas and recycling are intrinsically three-dimensional due to non-axisymmetric magnetic fields and toroidally inhomogeneous divertor plates. Additional complexity arises from a large variety of magnetic topologies encountered in configurations with different magnetic shear and complex magnetic structures ranging from small or large island chains to even coexisting slightly or strongly ergodic regions. For such open topologies standard magnetic coordinates do not exist. The approach used by the EMC3 code [1,2] is a Monte Carlo (MC) technique optimized for highly anisotropic 3D fluid transport processes in open magnetic topologies of arbitrary complexity. The parallel and cross-field transport dynamics of mass, momentum and energy are simulated by advancing MC "particles" along and across field lines through local orthogonal steps. Up to now, the EMC3 code, coupled self-consistently to the EIRENE code [3] for neutral transport, has been applied to W7-AS, W7-X, LHD, TEXTOR-DED and ITER start-up.

Presently, the NCSX magnetic boundary region [4,5] is being implemented in the code to start the investigation of the SOL transport properties for different configurations on the way to a first divertor design. A major step of this implementation is the construction of a 3D field-aligned grid extending toroidally half a field period and covering the radial SOL region of interest. At the boundary of the periodicity domain, field-line coordinates are transformed reversibly to the next domain by applying the RFLM technique [6]. This technique avoids both a numerical cross-field diffusion of the fast parallel transport and a radial accumulation of interpolation errors, which are critical issues especially in the high temperature region close to the LCFS.

2. NCSX boundary configuration

NCSX is a quasi-axisymmetric compact stellarator with three field periods, major radius of 1.4 m and aspect ratio of 4.4 [7]. The plasma configuration chosen for the present first application

francesco.sardei@ipp.mpg.de

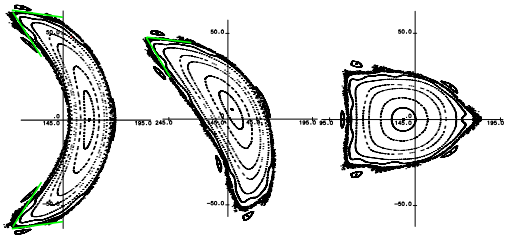

Fig. 1 NCSX configuration over half a field period (ϕ = 0°,30°,60°) with model target plates extending 1/4 of a field period at stellarator-symmetric positions.

(Fig. 1) has β = 4.1% and ι = 0.65 at the plasma edge (Fig. 2). The last closed flux surface (LCFS) is surrounded by a narrow weakly ergodic zone followed by an island chain at ι = 3/5 (Fig. 1). Outside this resonance strong radial field-line excursions to the wall indicate the end of the plasma region.

In a first approximation, four model target plates per field period are placed close to the LCFS at stellarator-symmetric positions. They are located at the tips of the bean-shaped cross section, which have the largest flux expansion (Fig. 1), and extend

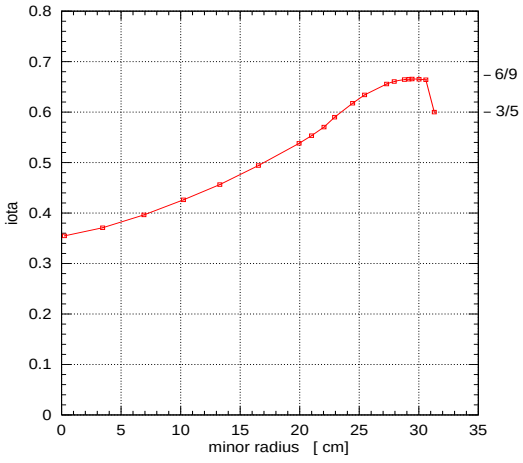

Fig. 2 ι profile for the configuration shown in Fig. 1.

1/4 of a field period starting at the bean-shaped symmetry plane (Fig. 1). The plates cut the LCFS at several toroidal positions, defining a limiter SOL with a highly inhomogeneous distribution of connection lengths (Fig. 3). Within a radial distance of about 3 cm from the LCFS, connection lengths L_c = 15-20 m, i.e. 5-7 field periods, dominate the SOL. The two relatively large up/down symmetric zones with $L_c \approx$ 3 m ≈ one field period in the upper and

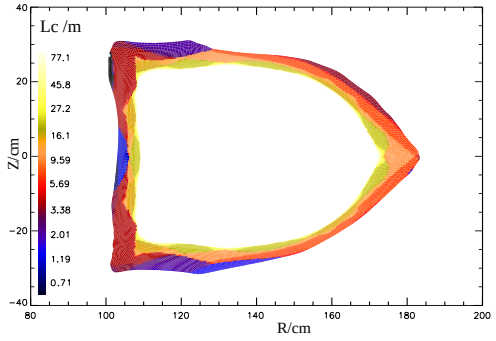

Fig. 3 Distribution of connection lengths as defined by the target plates shown in Fig. 1.

lower inboard corners of the ϕ = 60° symmetry plane (Fig. 3) are due to a local inward protrusion of the inboard plates into the core at toroidal angles of ϕ = 20°-25°. Deviations from up/down symmetry in the outermost short-L_c regions of the distribution are due to technical reasons and can be ignored.

3. Grid construction

In this section we shortly describe the structure of a typical 3D computational grid used by the EMC3-EIRENE code for stellarator-symmetric configurations and the basic steps of its construction. An extension to non-symmetric configurations is straightforward. Precomputed field lines are started from a fine 2D up/down symmetric grid of nested contours (Fig. 4) in the symmetry plane where the plates are located (bean-shaped plane of Fig. 1). The up/down symmetry of the grid is advisable because it allows a reduction of the computational domain to half a field period by a flux-coordinate representation of the boundary conditions and prevents an accumulation of radial interpolation errors [6]. The field lines are integrated numerically with high accuracy over half a field period and stored at fine-spaced toroidal intervals. The resulting two-parametric set of finite flux tubes covering the radial-poloidal region of interest contains all relevant information about the field structure including islands and ergodic regions. The radial and poloidal grid lines defining the cross-sections of the flux tubes become increasingly distorted in toroidal direction due to field shear. For high-shear devices, a strong distorsion may require a splitting of the flux-tube domain in two or more toroidal subdomains [6]. However, the distorsion does not affect the accuracy of the transport, as the flux-tube geometry does not enter the MC procedure, which is

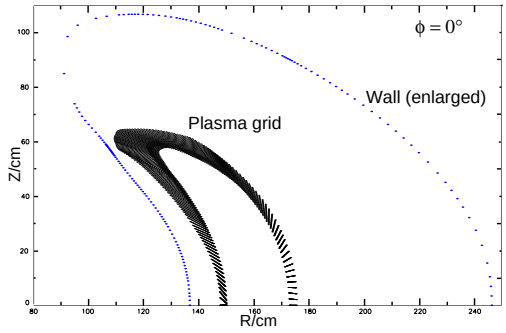

Fig. 4 Up/down symmetric cross-section of the computational grid at the starting plane. The wall (enlarged) is the radial boundary of the grid.

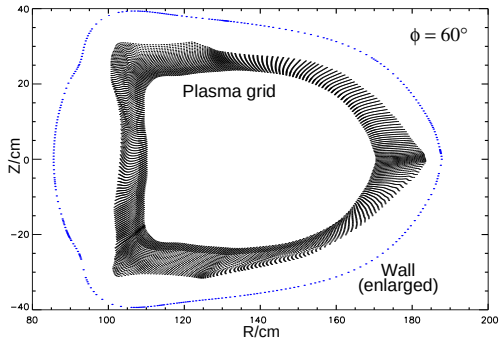

Fig. 5 Non-up/down symmetric cross section of the computational grid resulting from mapping of the starting grid (Fig. 4) over half a field period. The wall (enlarged) is the radial boundary of the grid.

based on local orthogonal displacements. In case of NCSX, the distortion is moderate and a single toroidal flux-tube domain is sufficient. However, the grid must be sufficiently fine to resolve small length scales of the plasma parameters especially near the target plates and to provide sufficient accuracy in the field-line interpolation.

The finite flux-tube SOL domain is bounded radially inwards by two flux surfaces close to the LCFS and outwards by a non-flux surface ("last surface") enclosing the relevant SOL plasma region (Figs. 4,5).

The two innermost flux surfaces are needed to correctly apply poloidal-dependent flux boundary conditions for the radial fluxes. They must be very close to each other and well defined, i.e. sufficiently sharp to form continuous, up/down symmetric toroidal surfaces in both planes of symmetry.

The "last surface" is the outer boundary of the finite flux-tube system defining the plasma computational domain. Together with the innermost flux surfaces, it should enclose a sufficiently large volume to completely cover the expected radial extension of the plasma SOL. If target plates are present, like in NCSX, the plasma SOL is bounded by the shadows of target plates catching most of the outflowing plasma. In the absence of target plates, like in LHD, the plasma SOL is bounded by flux tubes "hot-wired" to the wall, i.e. leading to wall contact within very short connection lengths. To a good starting approximation, the last surface could be identified with the radial boundary contour of a fine Poincaré distribution of particle orbits traced along field lines with cross-field diffusion. This could be the first step towards an optimization of the last surface, which eventually requires an iterative procedure based on the full plasma transport.

The space between the innermost and outermost surfaces is filled with nested surfaces obtained by radial interpolation between the bounding surfaces at the starting plane (Fig. 4).

In the present NCSX grid approximation, the last surface was obtained by adding a small toroidal field, thereby smoothing and shifting outwards the LCFS, and then radially extrapolating the basic island-free geometry of the edge configuration.

Since the 3D grid reflects the basic island-free topology of the boundary, it is not sensitive to small variations of rotational transform, ergodicity and edge island structures. Therefore, the same or a slightly modified grid may be used for different configurations.

Obviously, the 3D table of stored magnetic field used to integrate the field lines must fully cover the 3D plasma region. This requirement should be strictly controlled by the field-line tracing code to avoid errors which may be hardly detectable after the grid construction. Furthermore, both the table and flux-tube grids should be sufficiently fine to resolve magnetic flux conservation within a few %. This is an essential requirement not only for the intrinsic quality of the flux-tube system but also for the correct description of the parallel transport.

The wall represents the outer radial boundary of the 3D computational grid. No magnetic field is needed in the space between the wall and the plasma grid domain, this region being only populated by neutrals. Both the wall and the plasma facing components (target plates and baffles) are defined by their cross sections at ϕ = const planes.

Overlapping of grid cells arising from strong radial/poloidal distorsions, which may occur in the

whole computational grid up to the wall, must be avoided. Within the plasma grid it is sufficient to check for flux-tube overlapping at the boundary of the toroidal domain, whereas in the space between the plasma grid and the wall surface, overlapping needs to be checked at any toroidal position, as the poloidal distributions of the wall grid points are not magnetically interconnected in toroidal direction.

4. First EMC3 application

In the first test application of the EMC3 code to NCSX, only the 3D energy transport for electrons and ions were simulated, whereas the plasma density was kept fixed at n_e = 10^{19} m^{-3} throughout the computational domain. A power of P_{SOL} = 1.2 MW entering the SOL was equally distributed between ions and electrons, and the anomalous cross-field heat diffusivities were set to $\chi_e = \chi_i = 3$ m^2/s. These numbers have to be considered only as an example, which does not reflect realistic NCSX parameter values, as the subject of the present study is the code implementation, not an edge physics study. As expected from the L_c contour plot (Fig. 3), the relevant radial energy transport takes place in a narrow radial zone dominated by L_c = 15-20 m. The corresponding collisionality $\nu_e^* = L_c/\lambda_{ee}$ = 1-2 < 10 indicates that the SOL transport is in the sheath-limited convection regime with no significant

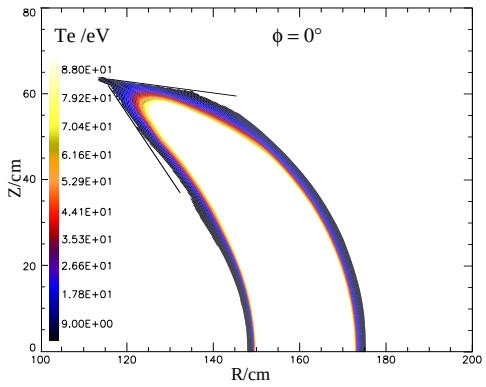

Fig. 6 Electron temperature distribution at the $\phi = 0°$ symmetry plane.

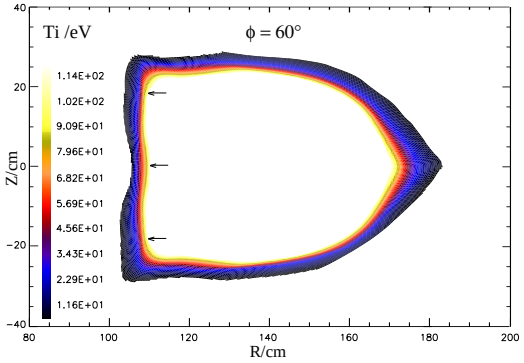

Fig. 7 Electron temperature distribution at the $\phi = 60°$ symmetry plane.

parallel temperature gradients [8]. The resulting temperature decay length (Figs. 6,7) is proportional to $\sqrt{L_c}$ and is estimated as $\lambda_T = \sqrt{2\chi_\perp \tau_{e//}}$ = 1-1.5 cm. A local energy sink in the two up/down symmetric SOL regions with $L_c \approx 3$ m (Fig. 3) is visible in Fig. 7 by comparing the radial T_e profiles at these two positions with that at the inboard midplane, which is governed by larger λ_T. The spatial distribution of T_i is similar as that of T_e, with T_i being about 10% higher throughout the SOL.

5. Next steps

Major technical steps still to be done towards a realistic description of the SOL transport in NCSX with the EMC3-EIRENE code are:

- improvement of the target-plate geometry
- improvement of the outermost plasma grid surface
- grid refinement near the plates
- activation of the full transport-equation system (particle, momentum, energy)
- activation of the self-consistent neutral gas transport
- tests of numeric convergence

Then, dedicated transport studies aiming, for example, at exploring the divertor potential of NCSX, could be started. Major tasks towards this goal would include

- characterizing the basic plasma transport properties for different 3D SOL configurations
- estimating the heat and particle deposition profiles on the target plates for different configurations and plate geometries
- optimizing the target-plate and baffle design with/without inboard plates with respect to wall protection, configuration flexibility, homogeneous load, neutral compression
- exploring the role of ergodicity and low-order edge islands for a divertor concept
- estimating the impurity retention capability in the SOL
- checking the sensitivity of the transport to low-

order resonances and ergodicity.

References

[1] Y. Feng, F. Sardei, J. Kisslinger, J. Nucl. Mater. **266-269,** 812 (1999)

[2] Y. Feng, F. Sardei, J. Kisslinger, P. Grigull, K. McCormick and D. Reiter, Contrib. Plasma Phys. **44** 1-3, 57 (2004)

[3] D. Reiter, M. Baelmans, and P. Boerner, Fusion Sci. Technol. **47**, 172 (2005)

[4] R. Maingi, et. al., Proc. of 33rd EPS on Plasma Physics and Controlled Fusion, Roma, Italy, June 19-23 (2006) paper P5.116

[5] T. Kaiser, et. al., Bull. Am. Phys. Soc. **51,** 39 (2006)

[6] Y. Feng, F. Sardei and J. Kisslinger, Phys. Plasmas **12,** 052505 (2005)

[7] M.C. Zarnstorff, et. al., Plasma Phys. Contr. Fusion **43,** A237 (2001)

[8] P.C Stangeby, The Plasma Boundary of Magnetic Fusion Devices, Plasma Physics Series, IoP 2000